Volume 62
Number 23
24 March 2026
Pages 6207–6420

ChemComm

Chemical Communications

rsc.li/chemcomm

ISSN 1359-7345

ROYAL SOCIETY OF CHEMISTRY

COMMUNICATION

Masumi Taki *et al.*

Programming the photoelasticity of hydrogels for label-free mechanosensing by a simultaneous birefringence-stress reader (SiBRe)

ChemComm

COMMUNICATION

Cite this: *Chem. Commun.*, 2026, **62**, 6314

Received 5th December 2025,
Accepted 3rd February 2026

DOI: 10.1039/d5cc06937h

rsc.li/chemcomm

Programming the photoelasticity of hydrogels for label-free mechanosensing by a simultaneous birefringence-stress reader (SiBRe)

Riku Katsuki,[a] Marc Eisenmann,[b] Shalika Singh,[c] Takayuki Tomaru[b] and Masumi Taki *[ad]

We present a strategy to program hydrogel photoelasticity using rationally designed force-transducing crosslinkers. Enabled by a simultaneous birefringence-stress reader (SiBRe), we show that stress-induced unfolding of flexible linkers can amplify the optical response, establishing a robust, dye-free platform for quantitative mechanosensing.

Visualizing molecular-scale forces is paramount for understanding the mechanical behavior and failure of polymeric materials. To this end, significant research has focused on utilizing mechanophores—molecular units that respond to mechanical stimuli by altering their optical or chemical properties—to probe these invisible forces at the molecular level.[1–3] Prevailing strategies have evolved from force-induced covalent bond cleavage in molecules like spiropyrans,[4–6] rhodamines[7–9] and Diels–Alder adducts[10,11] to more recent reversible approaches that leverage Förster resonance energy transfer (FRET) or the dissociation of supramolecular structures.[12,13]

These mechanophore-based approaches are increasingly embedded in soft polymer networks, particularly hydrogels, to visualize and quantify piconewton- to nanonewton-scale cellular forces.[14] Such tools, which are critical for mechanobiology's goal of understanding forces in three-dimensional environments, have been developed using a range of platforms and mechanisms, encompassing FRET in proteins,[15] DNA,[16,17] and rotaxanes,[18] excimer fluorescence,[19] strain-induced crystallization,[20] and host–guest systems.[21]

Despite these advancements, the application of these approaches in hydrogels for sensitive, quantitative force measurements suffers from significant limitations. The optical signal generated upon tension is often obscured by the material's pre-existing background fluorescence. Furthermore, achieving a substantial signal change frequently requires material deformations exceeding 300%, a range unsuitable for most biological systems.[15,20] These limitations highlight the need for an alternative sensing modality that does not rely on chemical reactions or fluorescence, but instead on a direct physical response to stress.

Stress-induced birefringence (*i.e.*, photoelasticity) provides a dye-free physical readout,[21] yet it has rarely been developed for quantitative sensing of small, cellular-scale forces in specific systems.[22–24] While hydrogels are typically optically isotropic, they can develop local anisotropy and thus exhibit birefringence when their internal polymer chains align in response to external stress.[25] Although birefringence measurements have been employed to analyze internal material anisotropy[26–28] and are finding applications in soft robotics,[21] these studies have predominantly focused on robust gels designed to withstand large forces. To the best of our knowledge, research utilizing birefringence as a quantitative sensor for small, cellular-scale forces remains scarce in synthetic hydrogels.

In this proof-of-concept study demonstrating quantitative mechanosensing *via* photoelastic response, we establish a strategy to molecularly program hydrogels using a custom-built simultaneous birefringence-stress reader (SiBRe; Fig. 1) that co-registers birefringence (Δn) and true stress (σ). Focusing on polyacrylamide (PAA) as a model hydrogel, we first validated the material's mechanical linearity to ensure quantitative reliability. While hydrogels generally exhibit hyperelastic nonlinearity or strain-stiffening at large deformations,[29] our tensile testing of the 12% (w/v) PAA matrix (crosslinker ratio 19 : 1) confirmed approximate linearity within the targeted low-stress range ($\sigma < 15$ kPa, corresponding to strain $\varepsilon < 0.25$) relevant to cellular forces (Fig. S2, SI). This linear approximation in the initial strain range is consistent with previous mechanical characterizations of PAA networks,[28] justifying the use of a

[a] *Department of Engineering Science, The Graduate School of Informatics and Engineering, The University of Electro-Communications (UEC), 1-5-1 Chofugaoka, Chofu, Tokyo 182-8585, Japan. E-mail: taki@pc.uec.ac.jp; Tel: +81-42-443-5980*
[b] *National Astronomical Observatory of Japan (NAOJ), 2-21-1 Osawa, Mitaka, Tokyo 181-8588, Japan*
[c] *Department of Physics, Institute of Science Tokyo, 2-12-1 Ookayama, Meguro, Tokyo 152-8551, Japan*
[d] *Institute for Advanced Science, UEC, Chofu 182-8585, Japan*

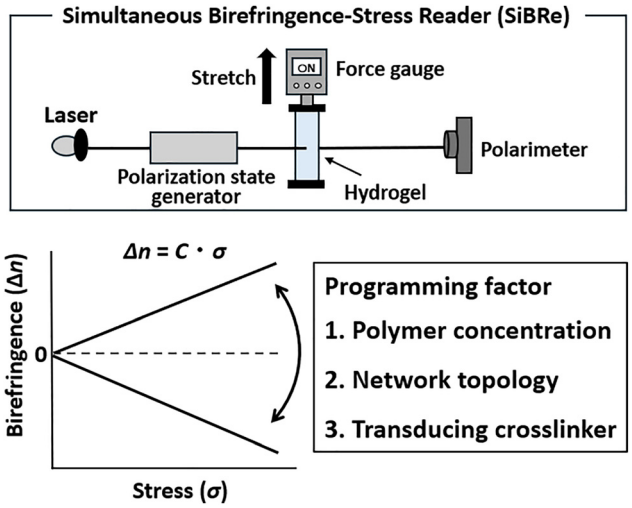

Fig. 1 Strategy for programming and quantitative readout of the photoelastic response. Top: A custom-built simultaneous birefringence-stress reader (SiBRe) acquires real-time, co-registered measurements of stress (σ) and birefringence (Δn) as a hydrogel sample is uniaxially stretched. For the details, see Fig. S1, SI. Bottom: The photoelastic response exhibits $\Delta n = C \times \sigma$, where the stress-optical coefficient (C) represents the sensitivity. We demonstrate that C can be rationally programmed by modulating three key factors: (1) polymer concentration, (2) network topology, and (3) the incorporation of force-transducing crosslinkers.

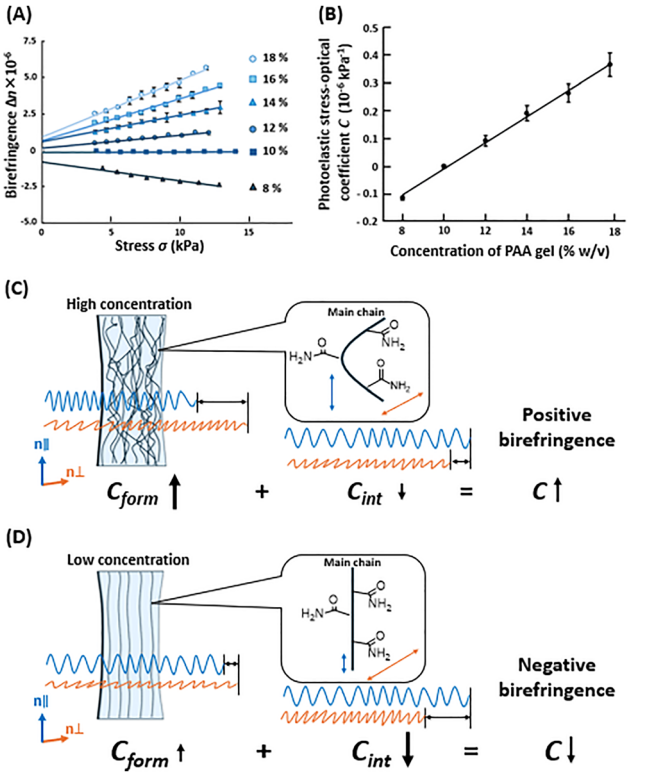

Fig. 2 Intrinsic photoelastic properties of polyacrylamide (PAA) gels. (A) Photoelastic response of PAA gels, revealing a concentration-dependent linear relationship between birefringence and stress. (B) Photoelastic stress-optical coefficient at different concentrations of acrylamide (8% to 18% w/v). Schematic representations of the proposed network topologies for (C) high-concentration gels showing positive form birefringence (C_{form}), where the polymer network dominates the optical response ($n_{\parallel} > n_{\perp}$), and (D) low-concentration gels showing negative intrinsic birefringence (C_{int}), driven by the perpendicular alignment of pendant amide groups ($n_{\perp} > n_{\parallel}$). Note: Positive ($\Delta n > 0$) and negative ($\Delta n < 0$) birefringence indicate the slow axis aligning parallel and perpendicular to stress, respectively.

constant stress-optical coefficient within this specific dynamic range. With the current sample geometry, SiBRe affords a practical stress resolution of $\sim$1 kPa (Fig. 2A and B). We note that this resolution is improvable; it is determined by the ratio of force sensor precision to the sample's cross-sectional area, allowing for higher sensitivity with larger samples (see SI for details).

We then employed SiBRe to characterize the intrinsic photoelasticity of the matrix, revealing that the stress-optical coefficient C of PAA reversed sign with concentration to cross zero near 10% w/v (Fig. 2A and B). This determination relied on the strict linearity observed in the small-stress regime (Fig. 2A), which is consistent with previous studies on viscoelastic hydrogels.[21] On the basis of standard polymer network theories, we attributed this transition to the competitive interplay between two distinct optical contributions: $C = C_{int} + C_{form}$.[30] Here, C_{int} represents the negative intrinsic birefringence ($n_{\perp} > n_{\parallel}$) arising from the perpendicular alignment of polymer chains, specifically the anisotropic amide side groups relative to the polymer backbone. Conversely, C_{form} denotes the positive form birefringence originating ($n_{\parallel} > n_{\perp}$) from the refractive index mismatch between the PAA network (n = 1.59) and water (n = 1.33)[31] due to structural inhomogeneities. At higher concentrations of PAA, the positive form birefringence arising from the deformation of loose, inhomogeneous networks dominates, as schematically depicted in Fig. 2C. However, as concentration decreases, the negative intrinsic birefringence from chain alignment becomes more pronounced (Fig. 2D), cancelling out the positive form component to yield a net zero optical response at $\sim$10% w/v.

Regardless of polymer concentration, our following data suggest that crosslinker functionality is the primary determinant of photoelastic sensitivity, following an empirical linear scaling relationship that we term "topological additivity." This topological contribution outweighs the limited effect of simply increasing crosslink density. Indeed, while varying crosslink density with the standard bifunctional Bis (f = 2) is common practice to tune mechanics, it yielded only marginal changes in the stress-optical coefficient C (Fig. 3B). This suggests that bifunctional linkers act merely as passive chain connectors.[32] In contrast, incorporating trifunctional (Tris, f = 3) and tetrafunctional (Tetra, f = 4) crosslinkers revealed that the photoelastic sensitivity scales linearly with crosslinker functionality f (Fig. 3A and B). We attribute the concentration-dependent decrease in C to enhanced stress transmission, which is significantly amplified by the network topology. Physically, by anchoring a greater number of polymer strands to a single node, the polyfunctional crosslinkers compel the connected chains to stretch cooperatively. This mechanism rationalizes the distinct

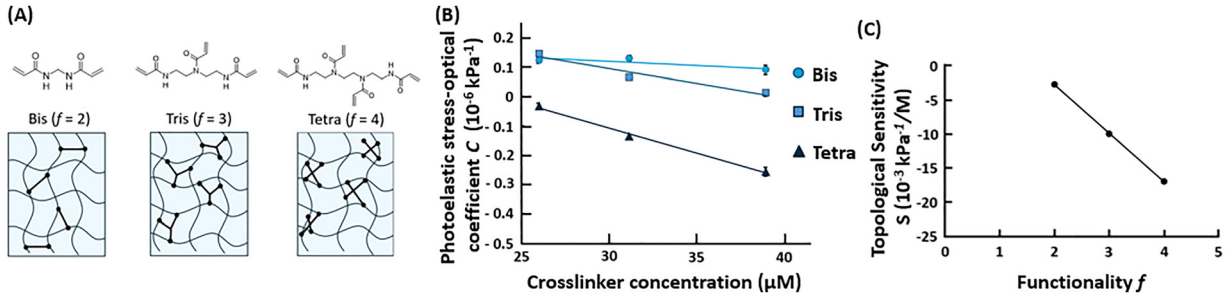

Fig. 3 Effect of crosslinker topology on the photoelastic response. (A) Chemical structures of the standard crosslinker (Bis, f = 2) and polyfunctional analogues (Tris, f = 3; Tetra, f = 4), alongside schematics of the resulting network topologies. (B) Dependence of the stress-optical coefficient (C) on the concentration of each crosslinker introduced into a 12% (w/v) PAA matrix. The slope of each line represents the topological sensitivity (S). (C) Discovery of topological additivity. The topological sensitivity (S) was plotted against the crosslinker functionality (f).

separation of values observed at higher concentrations, suggesting that high-order nodes act as active stress concentrators compared to the bifunctional crosslinker (*i.e.*, Bis). Notably, we found that the topological sensitivity (S)—defined as the gradient of C with respect to concentration—increases arithmetically with the number of branching arms; within error, S increases approximately linearly with f (Fig. 3C). This linear scaling highlights the role of high-order nodes function as rigid topological anchors. Unlike bifunctional linkers which allow significant conformational freedom, these multivalent nodes are inferred to suppress non-affine thermal fluctuations, promoting a transition to affine network behaviour,[33] and facilitate the cooperative alignment of the connected polymer strands with the macroscopic strain. Consequently, the network topology directly regulates the efficiency of stress-to-alignment transduction, establishing a programmable scaling relationship. This suggests that high-order nodes act as effective stress concentrators that amplify intrinsic chain alignment (C_{int}) while suppressing static inhomogeneities (C_{form}). Thus, the photoelastic response was established as a programmable property governed by the network topology.

To make a programmable hydrogel possessing a large and predictable negative C, we incorporated rationally-designed transducers (*i.e.*, force-transducing crosslinkers) into the near-zero-baseline 10% w/v PAA matrix (Fig. 4A and B). We hypothesize that stress-induced alignment of anisotropic benzene rings within each crosslinker unit, which transition from random orientations in the relaxed state to alignment with the principal stress direction, generates measurable optical anisotropy. Consistent with this mechanism, birefringence changed with crosslinker concentration; the induced birefringence scaled linearly with crosslinker loading (Fig. S3, SI), confirming tunable sensitivity and quantitative incorporation. Notably, the magnitude of the induced birefringence differed between the two crosslinkers. Crosslinker-1, which features a more conformationally flexible ethylene glycol linker than the single ether linkage in crosslinker-2, induced a significantly more negative photoelastic response (Fig. 4B). This observation suggests that the initial, pre-polymerized conformation of the crosslinker within the hydrogel network may play a crucial role. Molecular dynamics (MD) simulations provide a mechanistic rationale consistent with this hypothesis, suggesting that crosslinker-1 can adopt a compact, folded structure *via* intramolecular π-stacking, whereas crosslinker-2 more readily populates distorted conformations (Fig. 4C). We speculate such pre-organization could facilitate a more cooperative and substantial change in molecular alignment under strain, thereby amplifying the photoelasticity. These findings reveal that the intrinsic optical response of the PAA matrix can vary substantially and must be controlled when engineering sensitive hydrogel-based stress sensors.

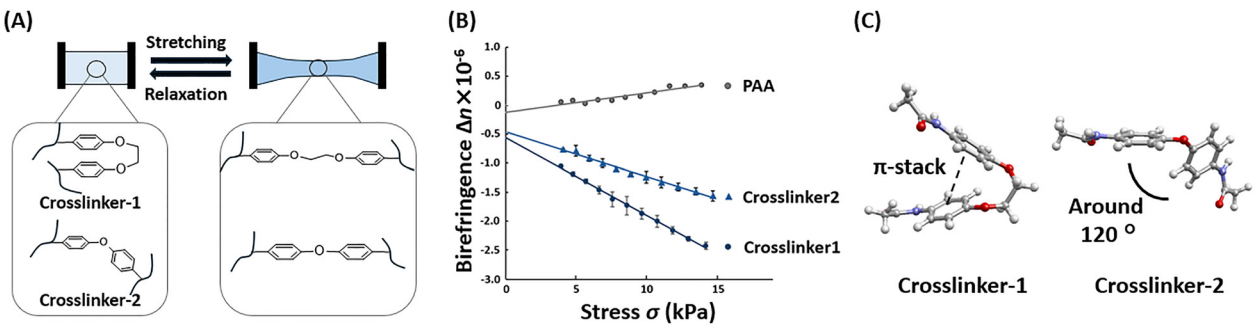

Fig. 4 Molecular engineering of a programmable photoelastic response. A large, predictable photoelastic response was imparted to a 10% w/v PAA gel—which had near-zero intrinsic birefringence—by incorporating rationally designed, force-transducing crosslinkers. (A) Chemical structures of the anisotropic crosslinkers. (B) Both crosslinkers induced substantial and predictable negative birefringence when copolymerized into a 10% w/v PAA matrix, which otherwise exhibited near-zero birefringence. Crosslinker-1 yielded a more significant response ($C_1 = -0.17 \times 10^{-6}$ kPa^{-1}) than crosslinker-2 ($C_2 = -0.11 \times 10^{-6}$ kPa^{-1}). (C) Molecular dynamics simulations predicted distinct minimum-energy conformations: crosslinker-1 favours a compact, π-stacked structure that may facilitate more cooperative alignment under strain, amplifying the photoelasticity.

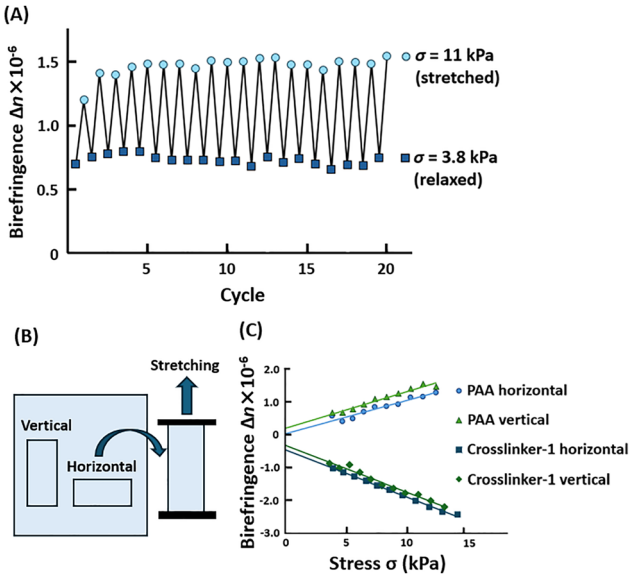

Fig. 5 The engineered hydrogel demonstrated excellent reversibility and directional independence. (A) The photoelastic response of PAA gel over 20 consecutive cycles of stretching (11 kPa) and relaxation (3.8 kPa). (B) Schematic of the directional-independence test, where samples were excised in orthogonal (*i.e.*, vertical and horizontal) directions from a single hydrogel slab. (C) Stress-birefringence plots for PAA (12% w/v) and crosslinker-1-incorporated gels cut in both orientations.

The reversibility and directional independence of the hydrogel photoelastic response were validated, confirming its capability as a stress sensor. The birefringence response remained stable over at least 20 cycles of stretching and relaxation, indicating elastic and reversible deformation within the tested range (Fig. 5A and Fig. S4, SI). Furthermore, the response was non-directional; samples excised in orthogonal directions (*i.e.*, vertical and horizontal) from a single gel slab showed identical C for both unmodified PAA and the crosslinker-1-incorporated one (Fig. 5B and C). This directional independence is consistent with a homogeneous network structure, ensuring a consistent sensor response regardless of force orientation. This direction-independent property is critical for resolving complex, multi-directional stress fields like those generated by living cells.

In conclusion, we have demonstrated a strategy to program the photoelastic response of hydrogels at the molecular level: by zeroing the matrix's intrinsic birefringence baseline and co-registering birefringence (Δn) and stress (σ) with SiBRe, force-transducing crosslinkers yield a large, reversible and non-directional photoelastic response suitable for microscale force sensing. We believe this research establishes a rationally tunable, calibration-ready foundation for future quantitative force mapping, thereby accelerating parallel advancements in material synthesis and optical instrumentation toward precision mechanobiology and mechanomedicine.[34,35]

Conflicts of interest

There are no conflicts to declare.

Data availability

All data supporting the findings of this study are included in the article and supplementary information (SI). Supplementary information: ref. 29, 36 and 37 are cited. See DOI: https://doi.org/10.1039/d5cc06937h.

Acknowledgements

This work was supported by JSPS KAKENHI grant (#23KJ0969, #24K00649, #24K21551), UEC-NAOJ internal grant, Ministry of Education, Culture, Sports, Science and Technology (MEXT) (220003). A part of this work was supported by "Advanced Research Infrastructure for Materials and Nanotechnology in Japan (ARIM)" of the MEXT; Proposal number JPMXP1225UE0028. R.K. acknowledges initial support from the UEC integrated PhD program (Open Innovation Course), which enabled a collaborative project in a completely different field of expertise—astronomical telescope calibration using birefringence measurement—that inspired new research ideas, as well as for the Grant-in-Aid for JSPS DC1 Research Fellows.

References

1 Y. Chen, G. Mellot, D. van Luijk, C. Creton and R. P. Sijbesma, *Chem. Soc. Rev.*, 2021, **50**, 4100.
2 J. Li, C. Nagamani and J. S. Moore, *Acc. Chem. Res.*, 2015, **48**, 2181.
3 A. L. Black, J. M. Lenhardt and S. L. Craig, *J. Mater. Chem.*, 2011, **21**, 1655.
4 T. Bercovici and E. Fischer, *J. Am. Chem. Soc.*, 1964, **86**, 5687.
5 G. Smets and F. de Blauwe, *Pure Appl. Chem.*, 1974, **39**, 225.
6 D. A. Davis, A. Hamilton, J. Yang, L. D. Cremar, D. Van Gough, S. L. Potisek, M. T. Ong, P. V. Braun, T. J. Martínez, S. R. White, J. S. Moore and N. R. Sottos, *Nature*, 2009, **459**, 68.
7 Z. Chen, J. A. M. Mercer, X. Zhu, J. A. H. Romaniuk, R. Pfattner, L. Cegielski, T. J. Martinez, N. Z. Burns and Y. Xia, *Science*, 2017, **357**, 475.
8 Z. Wang, Z. Ma, Y. Wang, Z. Xu, Y. Luo, Y. Wei and X. Jia, *Adv. Mater.*, 2015, **27**, 6469.
9 T. Wang, N. Zhang, J. Dai, Z. Li, W. Bai and R. Bai, *ACS Appl. Mater. Interfaces*, 2017, **9**, 11874.
10 A. R. Sulkanen, J. Sung, M. J. Robb, J. S. Moore, N. R. Sottos and G.-Y. Liu, *J. Am. Chem. Soc.*, 2019, **141**, 4080.
11 R. Göstl and R. P. Sijbesma, *Chem. Sci.*, 2016, **7**, 370.
12 Y. Sagara, M. Karman, E. Verde-Sesto, K. Matsuo, Y. Kim, N. Tamaoki and C. Weder, *J. Am. Chem. Soc.*, 2018, **140**, 1584.
13 Y. Sagara, M. Karman, A. Seki, M. Pannipara, N. Tamaoki and C. Weder, *ACS Cent. Sci.*, 2019, **5**, 874.
14 F. A. Soares and P. Besenius, *Org. Chem. Front.*, 2025, **12**, 3107.
15 M. Taki, T. Yamashita, K. Yatabe and V. Vogel, *Soft Matter*, 2019, **15**, 9388.
16 G. Creusen, R. S. Schmidt and A. Walther, *ACS Macro Lett.*, 2021, **10**, 671.
17 R. Merindol, G. Delechiave, L. Heinen, L. H. Catalani and A. Walther, *Nat. Commun.*, 2019, **10**, 528.
18 T. Muramatsu, S. Shimizu, J. M. Clough, C. Weder and Y. Sagara, *ACS Appl. Mater. Interfaces*, 2023, **15**, 8502.
19 Y. Sagara, H. Traeger, J. Li, Y. Okado, S. Schrettl, N. Tamaoki and C. Weder, *J. Am. Chem. Soc.*, 2021, **143**, 5519.
20 K. Suga, T. Yamakado and S. Saito, *J. Am. Chem. Soc.*, 2023, **145**, 26799.
21 J. Liu, W. Li, Y. She, S. Blanchard and S. Lin, *Adv. Mater.*, 2024, 2407925.
22 S. Sugita, E. Mizutani, M. Hozaki, M. Nakamura and T. Matsumoto, *Sci. Rep.*, 2019, **9**, 3960.
23 A. Curtis, L. S. Csaderova and G. Aitchison, *Biophys. J.*, 2007, **92**, 2255.

24 R. Alavi, O. Chancy, B. Trudel, L. Dewit, C. Luthold, L. Piquet, A. Akbarzadeh, M. Desjardins, S. Landrevile and F. Bordeleau, *Acta Biomater.*, 2025, **200**, 236.
25 D. Brewster, *Philos. Trans. R. Soc. London*, 1815, **105**, 29.
26 D. R. King, R. Takahashi, T. Ikai, K. Fukao, T. Kurokawa and J. P. Gong, *ACS Appl. Polym. Mater.*, 2020, **2**, 2350.
27 R. Takahashi, Z. L. Wu, M. Arifuzzaman, T. Nonoyama, T. Nakajima, T. Kurokawa and J. P. Gong, *Nat. Commun.*, 2014, **5**, 4490.
28 Z. L. Wu, D. Sawada, T. Kurokawa, A. Kakugo, W. Yang, H. Furukawa and J. P. Gong, *Macromolecules*, 2011, **44**, 3542.
29 C. G. Antipova, A. E. Krupnin, A. R. Zakirov, V. V. Pobezhimov, D. A. Romanenko, D. Y. Stolyarova, S. N. Chvalun and T. E. Grigoriev, *Polymers*, 2025, **17**, 737.
30 J. Bossart and H. C. Öttinger, *Macromolecules*, 1997, **30**, 5527.
31 Y. Xu and I. Teraoka, *Macromolecules*, 1999, **32**, 4596.
32 L. R. G. Treloar, *The Physics of Rubber Elasticity*, Clarendon Press, Oxford, 3rd edn, 1975.
33 T. Sakai, *Polym. J.*, 2014, **46**, 517.
34 Z. Liu, G. Chen, M. S. Jo, *et al.*, Mechanomedicine, *Nat. Rev. Bioeng.*, 2026, DOI: 10.1038/s44222-025-00391-6; G. M. O'Neill, C. Zhu, D.-H. Kim and J. Shin, Mechanomedicine: translating mechanical forces into therapeutic strategies, *APL Bioeng.*, 2025, **9**, 040401.
35 Y. Kalukula, G. Ciccone, D. Mohammed, A. Procès, M. Versaevel, A. Deridoux, L. Ergot, Z. Barbier, M. Mansy, R. Aucouturier, R. Tranzer, M. Surin, S. Gabriele and M. Luciano, *Sci. Adv.*, 2025, **11**, 31.
36 M. Eisenmann, S. Singh and M. Leonardi, *Opt. Lett.*, 2024, **49**, 3404.
37 S. Singh, M. Eisenmann, Y. Aso and K. Somiya, *Opt. Express*, 2025, **33**, 17462.

